Research Article | Vol. 27, No. 8 | 15 Apr 2019 | OPTICS EXPRESS 11547
Optics EXPRESS

Octave-wide supercontinuum generation of light-carrying orbital angular momentum

G. PRABHAKAR,[1] P. GREGG,[1] L. RISHOJ,[1] P. KRISTENSEN,[2] AND S. RAMACHANDRAN[1,*]

[1]*Boston University, 8 Saint Mary's St., Boston, MA 02215, USA*
[2]*OFS Fitel ApS, Brøndby, Denmark*
**sidr@bu.edu*

Abstract: Nonlinear frequency generation of light-carrying orbital angular momentum (OAM), which facilitates realization of on-demand, frequency-diverse optical vortices, would have utility in fields such as super-resolution microscopy, space-division multiplexing and quantum hyper-entanglement. In bulk media, OAM beams primarily differ in spatial phase, so the nonlinear overlap integral for self-phase matched $\chi^{(3)}$ processes remains the same across the 4-fold degenerate subspace of beams (formed by different combinations of spin and orbital angular momentum) carrying the same OAM magnitude. This indistinguishable nature of nonlinear coupling implies that supercontinuum generation, which substantially relies on self/cross-phase modulation, and Raman soliton shifting of ultrashort pulses typically results in multimode outputs that do not conserve OAM. Here, using specially designed optical fibers that support OAM modes whose group velocity can be tailored, we demonstrate Raman solitons in OAM modes as well as the first supercontinuum spanning more than an octave (630 nm to 1430 nm), with the entire spectrum in the same polarization as well as OAM state. This is fundamentally possible because spin-orbit interactions in suitably designed fibers lead to large effective index and group velocity splitting of modes, and this helps tailoring nonlinear mode selectivity such that all nonlinearly generated frequencies reside in modes with high spatial mode purity.

1. Introduction and background

Light-carrying orbital angular momentum (OAM) [1] has recently received tremendous attention due to potential applications in classical [2–4] and quantum communications, [5–7] super-resolution microscopy [8,9], manufacturing [10], sensing [11] and exo-planet detection [12]. While a majority of these investigations have considered the linear properties of OAM beams, their nonlinear optical properties have been less studied. For the case of second order ($\chi^{(2)}$) optical nonlinearities, reported investigations of spontaneous down-conversion, up-conversion and second harmonic generation [13–15] suggest that the behavior of OAM light beams shares the rules of conventional nonlinear optics, and thus appropriate phase matching with $\chi^{(2)}$ crystals results in desired nonlinear frequency generation. Corresponding studies of third order ($\chi^{(3)}$) optical nonlinearities, responsible for a host of effects ranging from Raman scattering to supercontinuum generation, however, present a more intricate picture. Propagation of an intense ultrashort pulse laser in an optical vortex state has been shown to lead to supercontinuum generation [16] that preserves phase singularities that are the hallmark of OAM beams, but the resultant mode content was distributed across a range of beams with different OAM magnitudes. In the limited case of optical fibers that support only the first OAM mode order (in addition to the Gaussian-shaped fundamental mode), it is possible to obtain clean Raman scattering into single, pure vector modes [17] because the unique polarization distribution of vector modes, in conjunction with the strong polarization-dependence of $\chi^{(3)}$ nonlinearities, dictates that strong nonlinear coupling is possible only to a mode that substantially resembles the pump mode (in intensity and polarization distribution).

#354648 https://doi.org/10.1364/OE.27.011547
Journal © 2019 Received 11 Dec 2018; revised 23 Feb 2019; accepted 4 Mar 2019; published 10 Apr 2019

Optics EXPRESS

This special case notwithstanding, a generalized methodology to nonlinearly frequency-convert, or obtain spectrally diverse, OAM beams with high spatial coherence and mode purity has not been possible, though doing so would be of great utility to a variety of applications that require on-demand OAM beams of different colors, for which the only broadband solutions require independent generation of white light that is then transformed with a wideband mode converter [18,19].

The electric field, $E(r, \phi, z)$ of an OAM mode in optical fibers is given by:

$$E(r,\phi,z) = F(r)\begin{Bmatrix}\sigma^{\pm}\exp(\pm iL\phi)\exp(\beta_{SOA}z-\omega t)\\ \sigma^{\pm}\exp(\mp iL\phi)\exp(\beta_{SOAA}z-\omega t)\end{Bmatrix} \quad (1)$$

where $F(r)$ represents the radial distribution of the electric field (which is substantially similar for modes of the same $|\mathcal{L}|$), $\mathcal{L}$ is the topological charge associated with an OAM of $\mathcal{L}\hbar$ per photon, ϕ is the azimuthal angle, $\sigma^{\pm}$ denotes the (circular) polarization states associated with a spin angular momentum (SAM) of $\pm\hbar$ per photon, and β is the propagation constant, related to the effective index, n_{eff}, of the mode by $\beta = 2\pi n_{eff}/\lambda$ (λ is the free-space wavelength). Note the subscripts of β, representing two degenerate spin-orbit aligned states (SOA) where the sign of $\mathcal{L}$ and σ are the same, and two degenerate spin-orbit anti-aligned states (SOAA) where these two quantities are opposite in sign, respectively. In bulk media, for a given magnitude $|\mathcal{L}|$ of OAM, $\beta_{SOA} = \beta_{SOAA}$, and modes with the four combinations of SAM and OAM are four-fold degenerate (in β or n_{eff}, and hence also in group velocity, group velocity dispersion (GVD) and higher-order dispersion terms). Third-order nonlinear coupling between different modes is governed by the field overlap integral

$$F_{j,k} = \int E_j^* E_k dA \quad (2)$$

where the subscript E_j and E_k denote the normalized fields associated with two different modes. From Eq. (2), it is immediately apparent that nonlinear interactions would have similar strengths when coupling modes of the same or opposite sign of $\mathcal{L}$ since their radial field profiles are nearly identical. This implies that nonlinear scattering (due to Raman or self/cross-phase modulation) from a "pump" mode in $\mathcal{L}$ would occur, with equal probabilities, to a mode with the same $\mathcal{L}$ as well as a mode with the opposite topological charge of $-\mathcal{L}$. In addition, as the pulses propagate, their envelopes continue to temporally overlap due to the aforementioned four-fold degeneracy, enabling the nonlinear interaction to build up. This explains why nonlinearly generated supercontinua of OAM beams in bulk media have, thus far, resulted in multimode outputs.

2. Nonlinear evolution of OAM beams in fibers

The situation is dramatically different in an optical fiber. Due to the confinement potential of the waveguide, SOA and SOAA modes have different propagation constants –a result of spin-orbit interactions in the presence of dielectric anisotropies [20]. We have previously shown that this spin-orbit effect can be exacerbated by fiber design, and lifting this degeneracy (i.e. making $|\beta_{SOA}-\beta_{SOAA}|$) large) avoids linear mode mixing during fiber propagation through lengths as long as 13 km [21]. In addition, angular momentum conservation rules dictate that even the degenerate orthogonally polarized modes do not mix in the linear regime [22]. Thus, in a suitably designed optical fiber, the four-fold degeneracy of OAM modes depicted in Eq. (1) reduces to two 2-fold-degenerate subspaces, and coupling even within the doubly degenerate modes is inhibited. The nonlinear overlap integral (Eq. (2), however, remains the same, and linear mode stability does not guarantee nonlinear mode selectivity. Here, we show that the aforementioned degeneracy-lifting criteria that enabled stable linear behavior of OAM modes in fibers also facilitates controllable nonlinear interactions for ultrafast pulses of OAM beams in fibers. Figure 1(a) illustrates this effect: for a spin-orbit aligned pump

Optics EXPRESS

$(+\mathcal{L},\sigma^{+})$ the nonlinearly generated spin-orbit aligned modes $(\pm\mathcal{L},\sigma^{\pm})$ substantially temporally overlap with the pump throughout the length of the fiber resulting in efficient nonlinear conversion. However, the spin-orbit anti-aligned modes $(\mp\mathcal{L},\sigma^{\pm})$ do not overlap with the pump since they have different group velocity compared to spin-orbit aligned pump (arising from the lifted degeneracy). In addition, SAM is conserved because of the well-known result that co-polarized nonlinear products have much higher gain than cross-polarized beams [23]. Thus, the conservation of OAM and SAM leads to the observation that the pump light launched in a single OAM state remains in the same state across the nonlinearly generated frequencies.

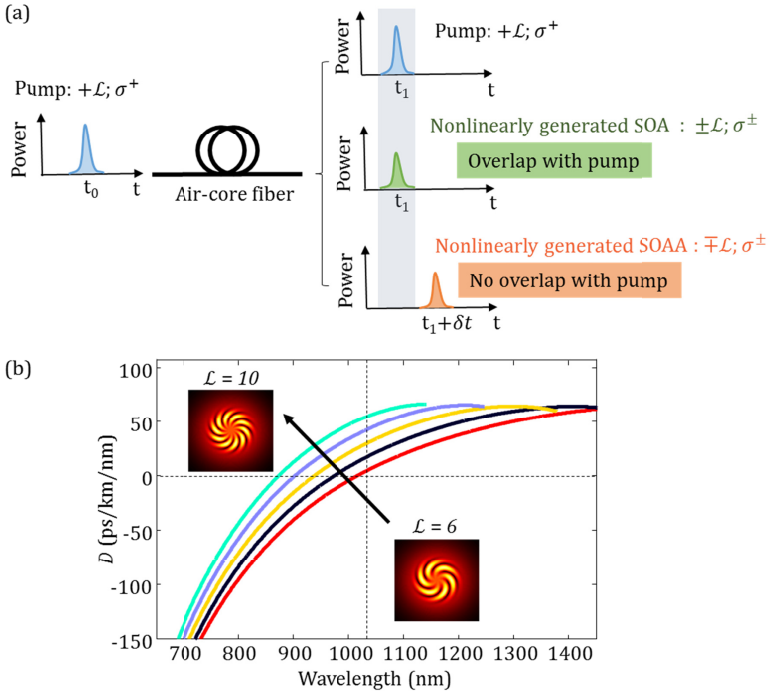

Fig. 1. (a) Schematic showing different group velocities for spin-orbit aligned (SOA) and spin-orbit anti-aligned (SOAA) states (b) Simulation of dispersion parameter D as a function of wavelength for $\mathcal{L}$ = 6 to 10 OAM states of air-core fiber, illustrating increasing dispersion as a function of OAM mode order.

There is another parameter that makes a fiber that supports OAM beams attractive for nonlinear optics. Group velocity dispersion (GVD), or equivalently the dispersion parameter D plays a critical role in the dynamics of $\chi^{(3)}$ mediated nonlinear optical processes. A key goal in engineering materials or waveguide structures for producing desired nonlinear effects is the achievement of anomalous GVD, or equivalently, the condition $D>0$ in the wavelength range of interest [24], since this automatically leads to phase matching, soliton formation and efficient supercontinuum generation [25]. Traditionally, this has been realized by engineering high optical confinement in waveguides, such as with Silicon nanophotonic circuits [26], or by photonic band gap tailoring, such as with photonic crystal fibers [27]. Dispersion D increases monotonically with mode order in any fiber – Fig. 1(b) shows the numerically simulated [28] dispersion D for the air-core fiber (described later) used in our experiments. Hence, OAM-carrying fibers represent a means of tuning the dispersion-zero simply by choice of the OAM mode order in which the pump beam is introduced.

Exploiting these attributes, we report the first demonstration of soliton self-frequency shifting (SSFS) and octave-wide supercontinuum generation of OAM light states in an optical

Optics EXPRESS

fiber. We find that both OAM and SAM are conserved across the generated supercontinuum bandwidth when a single OAM state is used as the pump, hence generating a spectrum in a vortex state that is temporally, spectrally as well as spatially coherent.

3. Experimental setup

We probe the nonlinear response of OAM-carrying light states using an ultrafast pump laser (Fig. 2(a): Calamar Cazadero with ~370 fs pulse width, 1030-nm center wavelength), since dispersive nonlinear effects are most readily apparent for pulses whose dispersion lengths (L_D ~7 m) are much greater than nonlinear lengths (L_{NL} ~0.02 m) [25]. A spiral phase front $exp[i\mathcal{L}\phi]$ introduced on the linearly polarized input pump beam using a spatial-light modulator (Hamamatsu LCOS-SLM x10468-08) is converted to circular polarization of the desired sign using a quarter-wave plate (Thorlabs WPQ05M) to select SOA or SOAA modes of the fiber. The fiber used in our experiments comprises a 6 μm diameter air core surrounded by a 6 μm high-index guiding ring [Fig. 2(b)] – a design known for conserving OAM and SAM (hence, total AM) upon linear light propagation [29]. We confirm this by analyzing the output mode images on a camera (Thorlabs DCC1645C for 600-1100 nm and Allied Vision Technologies "Goldeye" for 1100-1500 nm) after a polarization beam displacer (Thorlabs WP10), which shows that at low input power levels (before the onset of any nonlinearities), all the power remains in the same polarization state as that of the input [< 10% power in the orthogonal polarization bin shown in Fig. 2(d) compared to the main polarization σ^+ bin shown in Fig. 2(c)].

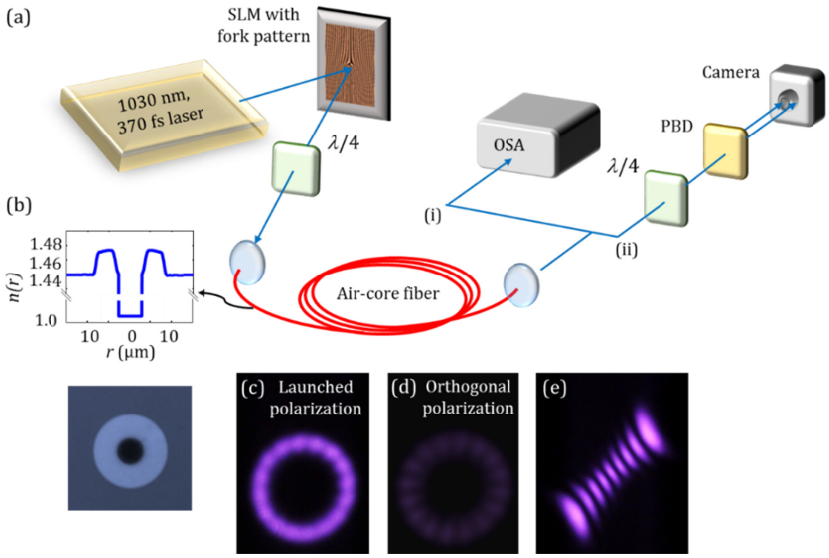

Fig. 2. (a) Experimental setup used for nonlinear frequency generation in 1-m long air-core fiber. The laser source emits 370 fs pulses at 1030 nm wavelength, which are coupled into the fiber after conversion into the desired OAM mode using an SLM. The output is characterized by sending it to either OSA or camera [branch *(i)* or *(ii)*]. PBD: polarizing beam displacer, λ/4: quarter waveplate, SLM: spatial light modulator, OSA: optical spectrum analyzer. (b) The measured refractive index profile (top) and fiber facet image (bottom) of the OAM supporting fiber used for the experiments. (c), (d) Output mode images from the fiber in the launched and its orthogonal polarization bin, respectively, at a power level before onset of nonlinearities, demonstrating the polarization-maintaining nature of OAM modes in this fiber. (e) Hermite-Gaussian-like mode image in the launched polarization state obtained by passing the output through a tilted lens. The number of singularities (8 in the figure) denotes value of ($|\mathcal{L}|$ = 8 in figure) – same as pump $|\mathcal{L}|$, indicating OAM preservation in the linear regime, in this fiber.

Optics EXPRESS

In addition, by adding a titled lens at the output, one can discern the value of the OAM state by counting the number of singularities of the resultant Hermite-Gaussian beam [30]. Figure 2(e) confirms that the output beam has the same topological charge as the input ($\mathcal{L} = +8$ in the case of the measurement illustrated in the figure, and we ensure this to be the case for all launched modes whose nonlinear properties were studied). By mode converting and performing image analysis on the output beam (see discussion related to Fig. 5 in Section 4), we infer that the mode purity at the output of the fiber is > 95%. Dielectric bandpass filters (Thorlabs FB; 10 nm full width half maximum) were used at the output to probe the nonlinear products at desired wavelength. The output spectra were measured using an optical spectrum analyzer (Ando 6317B).

4. Results

Figure 3 shows the output spectrum as input pump power is increased for a 1-m sample of the air-core fiber in the (a) $\mathcal{L} = +8$; σ^+ and (b) $\mathcal{L} = +7$; σ^+ (SOA) modes, respectively. For the lowest input power level (0.17 kW peak power coupled into fiber for $\mathcal{L} = +8$; σ^+), only linear propagation occurs and the output spectrum (blue curve) resembles that of the input pump. As the pump power is increased, we observe (red curve) the formation of a fundamental soliton ($N = 1$) that spectrally shifts away from the pump due to SSFS. As the peak power is increased further (to 52.8 kW, green curve), the soliton shifts to redder wavelengths, with a clear formation of a second soliton near the pump due to soliton fission. We also observe the concurrent formation of Cerenkov radiation at ~750 nm due to interactions with the shifted soliton at 1175 nm, resulting from the fact that the dispersion-zero wavelength for this mode is at ~925 nm (see Fig. 1(b) for relation between D and OAM content). Further increasing the input power shifts the soliton to even longer wavelengths, leading to multiple soliton fission events, eventually creating a broad spectrum that is clamped at ~1430 nm (pink curve at 220.1 kW launched peak power). The clamping occurs because the $\mathcal{L} = 8$ mode cuts off in our fiber at this wavelength (as confirmed via mode simulations). The measured energy in the furthest shifted fundamental soliton centered at ~1410 nm is 3.5 nJ. The experiments using $\mathcal{L} = +7$; σ^+ pump shows similar behavior with the fundamental soliton clamping at 1450 nm [Fig. 3(b)].

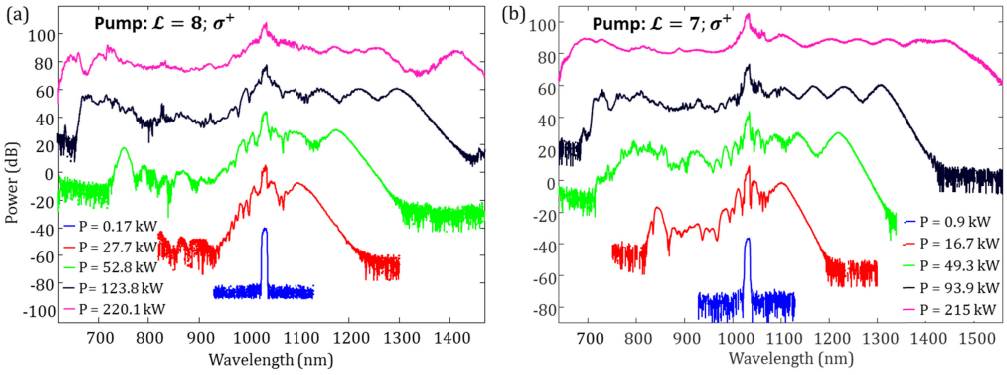

Fig. 3. Spectra showing soliton self-frequency shifting in (a) $\mathcal{L} = 8$ and (b) $\mathcal{L} = 7$ OAM state of the air-core fiber. The different spectra are obtained by increasing the peak power P coupled into the fiber. The spectra are offset from each other by 30 dB for clarity.

In Fig. 4(a), we show the spectrum measured at the fiber output when 373.8 kW of peak power is coupled into the $\mathcal{L} = 8$ mode. The spectrum spans more than an octave, from ~630 nm to ~1430 nm. The power in the supercontinuum at the fiber output was measured to be

Optics EXPRESS

356.9 kW, similar to the launched power, indicating negligible propagation or nonlinear losses.

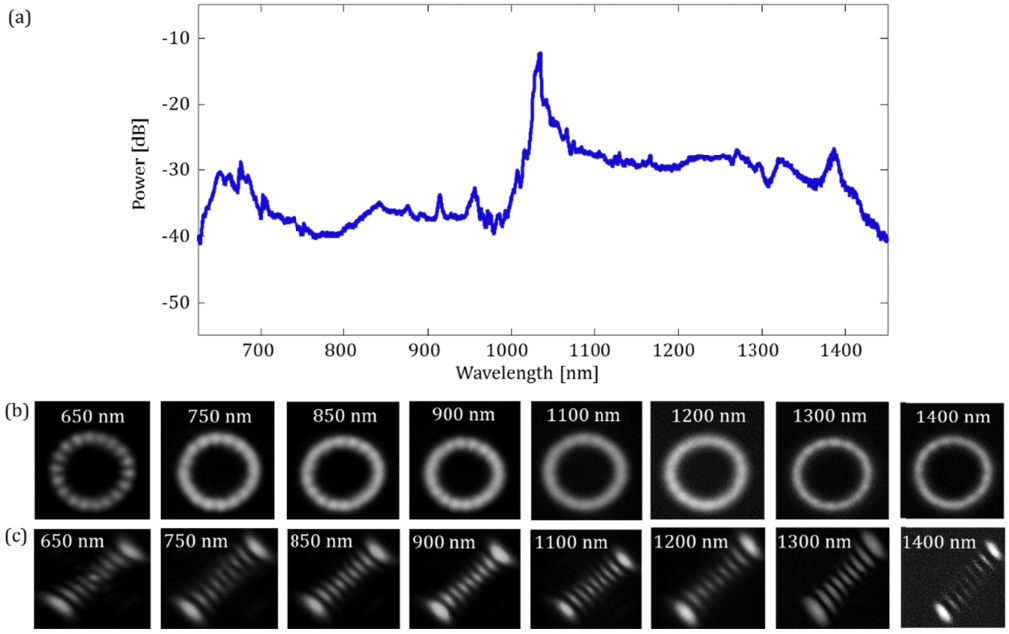

Fig. 4. (a) Measured supercontinuum spectrum in the $\mathcal{L}=8$ mode of the air-core fiber. (b) Output mode images in the launched polarization state at different wavelengths. (c) Hermite-Gaussian like mode images at different wavelengths of the supercontinuum, obtained using the method described in Fig. 2(e), confirming that the launched OAM mode order ($\mathcal{L}=8$) is maintained across the nonlinearly generated frequencies.

The spectra in Figs. 3 and 4(a) suggest that the nonlinear dynamics of ultrashort pulses in these fibers (wavelengths at which solitons form, their rate of shifting, onset and wavelength of Cerenkov radiation, and the extent of supercontinuum generation) follow that of a gedanken single mode waveguide with the given dispersion profile even though the fiber is itself multimoded. But spectra alone do not inform the output mode content, and we perform the same mode characterization measurements described for the low power linear regime [as per Fig. 2(e)] for the nonlinearly generated frequencies after spectrally slicing it with bandpass filters (FWHM ~10 nm) across the entire supercontinuum spectrum. Figure 4(b) shows the output mode image in the polarization bin in which light was initially launched into the fiber – the clean donut shaped mode images across the entire octave of the spectrum suggests the output to be in a pure OAM state. Figure 4(c) shows the corresponding output images after mode transformation using a tilted lens [similar to the characterization of the linear mode shown in Fig. 2(e)] – the distinct singularities in this image suggest that the output of the fiber in the launched polarization bin remains in the $\mathcal{L}$ = 8 mode (same as input pump) across the entire spectral range. However, mode images only provide a qualitative measure of mode purity since the interference between different OAM states on the camera depends strongly on the spectral bandwidth of the filtered source.

To quantify the output mode purities, we systematically characterize the mode-content using the setup shown in Fig. 5(a). The fiber output is passed through a spectral bandpass filter (tuned across the wavelength range, same as that in Fig. 4) and then a q = 3 q-plate, a device that converts the SOA $|\mathcal{L}|$ = 8 states to $|\mathcal{L}|$ = 14 ($\Delta L = 2q$), and the SOAA $|\mathcal{L}|$ = 8 states to $|\mathcal{L}|$ = 2 [31]. A circular polarization beam-splitter, comprising a quarter wave-plate and polarizing beam displacer, is used to separately evaluate the resultant images in the

Optics EXPRESS

launched polarization state as well as the orthogonal polarization state, respectively. Spatial integration of the camera intensity pattern across the two images reveals that the power ratio in the launched, versus the orthogonal polarization bins remains 6 dB (i.e. 75% power remain in the launched polarization state) across the spectrum [Fig. 5(c)]. This confirms the polarization (hence SAM) preserving behavior of the nonlinear process. Within the launched polarization bin, the relative modal content in SOA and SOAA is found by utilizing the fact that the $|\mathcal{L}|$ = 14 OAM state (converted from $|\mathcal{L}|$ = 8 SOA) diffracts more than the $|\mathcal{L}|$ = 2 state (converted from $|\mathcal{L}|$ = 8 SOAA) in free-space, as shown in Fig. 5(b); hence, the relative powers in the desired mode with respect to other modes is found by spatial integration of the four spatially separated regions (Region 1 corresponding to $|\mathcal{L}|$ = 14 and Region 3 corresponding to $|\mathcal{L}|$ = 2, and Region 2 and 4 composed of power in all other parasitic modes). Using this method, we find that the mode purity is better than 13 dB (>95%) across the spectral bandwidth [Fig. 5(d)]. This confirms that the dominant OAM content at all the nonlinearly generated frequencies is same as the launched pump state. We additionally confirm that both OAM and polarization are preserved across the generated supercontinuum when $\mathcal{L}$ = + 7; σ^+ state is used as the pump, indicating that the phenomenon is not dependent on OAM charge of the pump.

The measurement technique to discern mode purity above rests on two assumptions, both of which we show to be valid: (a) the intensity profiles of modes of the same, first, radial order (the primary mode orders used for the pump and probed in this experiment) need to be similar across different order of $\mathcal{L}$. This is substantially true for the air core fibers used in our experiments. In contrast to free-space or bulk media, the intensity profiles of modes with different $\mathcal{L}$ depends weakly on $\mathcal{L}$, because the high index contrast of the waveguide offering confinement plays the dominant role here. (b) power in other radial mode orders is assumed to be negligible. This validity of this assumption arises from the fact that intensity line cuts of the near field profiles all OAM modes exiting from our fiber [see Fig. 5(e)] match very well with simulated intensity profiles for our fiber – we find that an intensity overlap integral between the two yield 98% coincidence. Moreover, theoretically constructed intensity profiles assuming incoherent addition with other radial orders shows that obtaining such a high overlap would have meant that the other radial mode orders would have a maximum of 0.5% power, which is indeed negligible.

5. Discussion, summary and conclusions

These experiments reveal an interesting and highly useful attribute of nonlinear optics with OAM fiber modes – all nonlinear products arising from ultrafast pulse nonlinear effects conserve both polarization and OAM. Recall that this is fundamentally due to the effect of spin-orbit interactions in the air-core fiber, which results in group-velocity walk-off between spin-orbit aligned and anti-aligned states. Hence, self-phase matched nonlinear effects, such as Raman scattering or supercontinuum generation, with OAM beams can achieve high spatial coherence only in media that offer optical confinement with cylindrical symmetry, such as optical fibers or whispering gallery modes in ring resonators, but not in bulk media, where non-exclusive nonlinear coupling occurs.

Optics EXPRESS

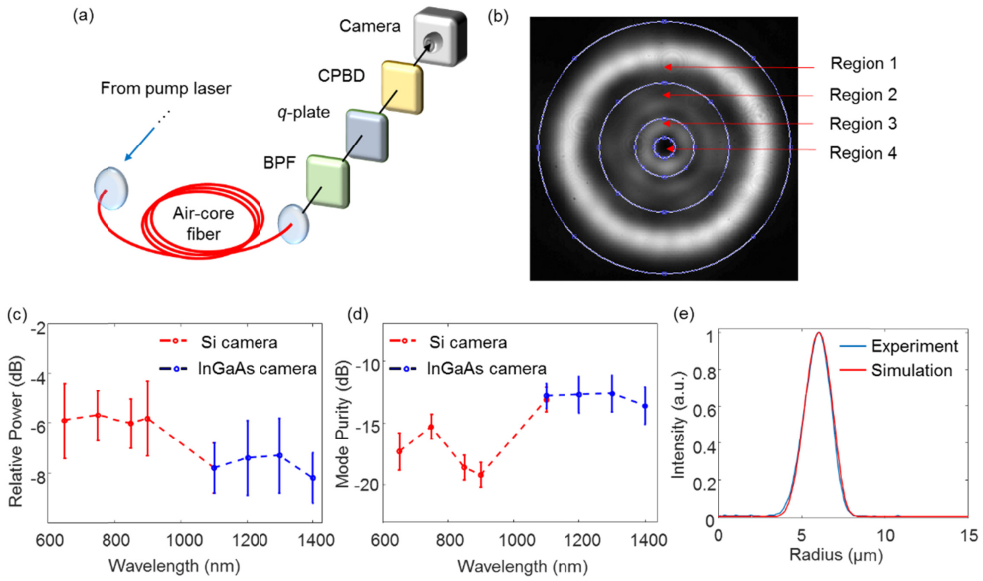

Fig. 5. (a) Setup to characterize mode purity at the fiber output using *q*-plate, bandpass filter (BPF), circular polarization beam displacer (CPBD) and camera at different wavelengths across the spectrum for $\mathcal{L} = 8$ mode shown in Fig. 4(a). (b) Representative output mode image in the launched polarization bin at $\lambda = 1400$ nm after mode-conversion using the *q*-plate. (c) Relative power in the launched polarization compared to the orthogonal polarization across wavelengths. (d) Mode purity measurements versus wavelength, in launched polarization bin (e) Experimental intensity line-cut of nonlinearly generated $\mathcal{L} = 8$ mode at 650 nm [mode image shown in Fig. 4(b)], compared with simulated intensity profile of the same mode.

In addition, control of OAM content in an optical fiber enables control of dispersion, a key parameter of interest in third-order nonlinear optics. This has two implications: (a) controlling OAM content, rather than mode size, as is typically done with high-confinement fundamental-mode waveguide nonlinear optics (either on-chip or fiber-based), enables achieving anomalous dispersion at the wavelength of choice – hence OAM content control would enable waveguide-based nonlinear optics in any spectral range in which an OAM fiber is transparent; (b) this dispersive control is independent of the effective area of the mode (which, at ~150 μm^2 in these experiments, is an order of magnitude larger than those of high-confinement fundamental-mode fibers commonly used for supercontinuum generation). Thus, the power spectral density of supercontinua produced by OAM beams in fibers can be an order of magnitude higher than that possible in conventional fibers.

In summary, we demonstrate multiple spatially selective and coherent ultrashort pulse nonlinear effects such as Raman soliton shifting and supercontinuum generation with OAM states of light, for the first time. The enabler is a suitably designed OAM supporting fiber, whose physics, related to spin-orbit interactions and dispersive behavior related to the rate of light's twist, yields record bandwidth (greater than an octave) frequency generation in a single, desired polarization as well as OAM state. Hence, third-order ultrashort pulse nonlinear optics with OAM beams in fibers is not only useful for the generation of spectrally diverse OAM beams for applications such as spectrally-diverse super-resolution nanoscopy and hybrid space-division multiplexing, it also provides an attractive wavelength-agnostic and power scalable platform to perform guided-wave nonlinear optics.

Optics EXPRESS

Funding

National Science Foundation (NSF) (ECCS-1610190); Air Force Office of Scientific Research (AFOSR) BRI program (FA9550-14-1-0165); Office of Naval Research (ONR) MURI (N00014-13-1-0627) and D&I (N00014-17-1-2519) programs.

Acknowledgments

The authors would like to acknowledge A. Rubano and L. Marrucci for manufacturing the *q*-plates used in the experiments.

Disclosures

The authors declare that there are no conflicts of interest related to this article.

References

1. A. M. Yao and M. J. Padgett, "Orbital angular momentum: origins, behavior and applications," Adv. Opt. Photonics **3**(2), 161–204 (2011).
2. J. Wang, J.-Y. Yang, I. M. Fazal, N. Ahmed, Y. Yan, H. Huang, Y. Ren, Y. Yue, S. Dolinar, M. Tur, and A. E. Willner, "Terabit free-space data transmission employing orbital angular momentum multiplexing," Nat. Photonics **6**(7), 488–496 (2012).
3. N. Bozinovic, Y. Yue, Y. Ren, M. Tur, P. Kristensen, H. Huang, A. E. Willner, and S. Ramachandran, "Terabit-scale orbital angular momentum mode division multiplexing in fibers," Science **340**(6140), 1545–1548 (2013).
4. B. Ung, P. Vaity, L. Wang, Y. Messaddeq, L. A. Rusch, and S. LaRochelle, "Few-mode fiber with inverse-parabolic graded-index profile for transmission of OAM-carrying modes," Opt. Express **22**(15), 18044–18055 (2014).
5. A. Mair, A. Vaziri, G. Weihs, and A. Zeilinger, "Entanglement of the orbital angular momentum states of photons," Nature **412**(6844), 313–316 (2001).
6. S. Gröblacher, T. Jennewein, A. Vaziri, G. Weihs, and A. Zeilinger, "Experimental quantum cryptography with qutrits," New J. Phys. **8**(5), 75 (2006).
7. L. Marrucci, E. Karimi, S. Slussarenko, B. Piccirillo, E. Santamato, E. Nagali, and F. Sciarrino, "Spin-to-orbital conversion of the angular momentum of light and its classical and quantum applications," J. Opt. **13**(6), 064001 (2011).
8. R. Dorn, S. Quabis, and G. Leuchs, "Sharper focus for a radially polarized light beam," Phys. Rev. Lett. **91**(23), 233901 (2003).
9. T. A. Klar, E. Engel, and S. W. Hell, "Breaking Abbe's diffraction resolution limit in fluorescence microscopy with stimulated emission depletion beams of various shapes," Phys. Rev. E Stat. Nonlin. Soft Matter Phys. **64**(6 Pt 2), 066613 (2001).
10. A. V. Nesterov and V. G. Niziev, "Laser beams with axially symmetric polarization," J. Phys. D **33**(15), 1817–1822 (2000).
11. M. P. J. Lavery, F. C. Speirits, S. M. Barnett, and M. J. Padgett, "Detection of a spinning object using light's orbital angular momentum," Science **341**(6145), 537–540 (2013).
12. G. Foo, D. M. Palacios, and G. A. Swartzlander, Jr., "Optical vortex coronagraph," Opt. Lett. **30**(24), 3308–3310 (2005).
13. A. Vaziri, J.-W. Pan, T. Jennewein, G. Weihs, and A. Zeilinger, "Concentration of higher dimensional entanglement: qutrits of photon orbital angular momentum," Phys. Rev. Lett. **91**(22), 227902 (2003).
14. B. Sephton, A. Vallés, F. Steinlechner, T. Konrad, J. P. Torres, F. S. Roux, and A. Forbes, "Spatial mode detection by frequency up-conversion," arXiv 1811.02632 (2018).
15. K. Dholakia, N. B. Simpson, M. J. Padgett, and L. Allen, "Second-harmonic generation and the orbital angular momentum of light," Phys. Rev. A **54**(5), R3742–R3745 (1996).
16. D. N. Neshev, A. Dreischuh, G. Maleshkov, M. Samoc, and Y. S. Kivshar, "Supercontinuum generation with optical vortices," Opt. Express **18**(17), 18368–18373 (2010).
17. S. Ramachandran, C. Smith, P. Kristensen, and P. Balling, "Nonlinear generation of broadband polarisation vortices," Opt. Express **18**(22), 23212–23217 (2010).
18. Z. Zhao, J. Wang, S. Li, and A. E. Willner, "Metamaterials-based broadband generation of orbital angular momentum carrying vector beams," Opt. Lett. **38**(6), 932–934 (2013).
19. N. Radwell, R. D. Hawley, J. B. Götte, and S. Franke-Arnold, "Achromatic vector vortex beams from a glass cone," Nat. Commun. **7**(1), 10564 (2016).
20. S. Ramachandran and P. Kristensen, "Optical vortices in fiber," Nanophotonics **2**(5-6), 455–474 (2013).
21. P. Gregg, P. Kristensen, and S. Ramachandran, "13.4km OAM state propagation by recirculating fiber loop," Opt. Express **24**(17), 18938–18947 (2016).
22. P. Gregg, P. Kristensen, and S. Ramachandran, "Conservation of orbital angular momentum in air-core optical fibers," Optica **2**(3), 267–270 (2015).
23. R. W. Boyd, *Nonlinear Optics*, 3th Ed. (Academic Press, 2008).

Optics EXPRESS

24. J. M. Dudley, G. Genty, and S. Coen, "Supercontinuum generation in photonic crystal fiber," Rev. Mod. Phys. **78**(4), 1135–1184 (2006).
25. G. P. Agrawal, *Nonlinear Fiber Optics*, 5th Ed. (Academic Press, 2015).
26. A. C. Turner, C. Manolatou, B. S. Schmidt, M. Lipson, M. A. Foster, J. E. Sharping, and A. L. Gaeta, "Tailored anomalous group-velocity dispersion in silicon channel waveguides," Opt. Express **14**(10), 4357–4362 (2006).
27. J. C. Knight, J. Arriaga, T. A. Birks, A. Ortigosa-Blanch, W. J. Wadsworth, and P. S. J. Russell, "Anomalous dispersion in photonic crystal fiber," Photon. Tech. Lett. **12**(7), 807–809 (2000).
28. M. E. V. Pedersen, P. Kristensen, L. Gruner-Nielsen, and K. Rottwitt, "Impact of the scalar approximation on the prediction of the group velocity dispersion," J. Lightwave Technol. **29**(21), 3129–3134 (2011).
29. S. Ramachandran, P. Gregg, P. Kristensen, and S. E. Golowich, "On the scalability of ring fiber designs for OAM multiplexing," Opt. Express **23**(3), 3721–3730 (2015).
30. P. Vaity, J. Banerji, and R. P. Singh, "Measuring the topological charge of an optical vortex by using a tilted convex lens," Phys. Lett. A **377**(15), 1154–1156 (2013).
31. L. Marrucci, C. Manzo, and D. Paparo, "Optical spin-to-orbital angular momentum conversion in inhomogeneous anisotropic media," Phys. Rev. Lett. **96**(16), 163905 (2006).